Published in final edited form as:
Methods. 2010 March ; 50(3): 157–165. doi:10.1016/j.ymeth.2009.10.003.

Rhesus Macaque Brain Morphometry: A Methodological Comparison of Voxel-Wise Approaches

Donald G. McLaren[1,2,3], **Kristopher J. Kosmatka**[1,3], **Erik K. Kastman**[1,3], **Barbara B. Bendlin**[1,3], and **Sterling C. Johnson**[1,3]

[1] Geriatric Research Education and Clinical Center, Wm. S. Middleton Memorial Veterans Hospital, Madison, WI 53705, USA

[2] Neuroscience Training Program, University of Wisconsin, Madison, WI 53706. USA

[3] Department of Medicine, University of Wisconsin, Madison, WI, 53705 USA

Abstract

Voxel-based morphometry studies have become increasingly common in human neuroimaging over the past several years; however, few studies have utilized this method to study morphometry changes in non-human primates. Here we describe the application of voxel-wise morphometry methods to the rhesus macaque (*Macaca mulatta*) using the 112RM-SL template and priors (McLaren et al. 2009) and as an illustrative example we describe age-associated changes in grey matter morphometry. Specifically, we evaluated the unified segmentation routine implemented using Statistical Parametric Mapping (SPM) software and the FMRIB's Automated Segmentation Tool (FAST) in the FMRIB Software Library (FSL); the effect of varying the smoothing kernel; and the effect of the normalization routine. We found that when studying non-human primates, brain images need less smoothing than in human studies, 2–4mm FWHM. Using flow field deformations (DARTEL) improved inter-subject alignment leading to results that were more likely due to morphometry differences as opposed to registration differences.

Keywords

rhesus macaque; MRI; morphometry; *Macaca mulatta*; brain mapping; aging; non-human primates

1. Introduction

In vivo brain imaging studies of grey matter morphometry in aging (Brickman et al., 2007a; Brickman et al., 2007b; Giorgio et al., 2008; Good et al., 2001; Kalpouzos et al., 2007; Sowell et al., 2004a; Sowell et al., 2004b) and neurological disease (Beyer et al., 2007; Ceccarelli et al., 2008; Chetelat et al., 2008; Hamalainen et al., 2008; Honea et al., 2008; Meisenzahl et al., 2008; Wolf et al., 2007; Yoo et al., 2008) in humans have provided a wealth of new information due to the accessibility of voxel-wise analysis methods. Previously, morphometry studies utilized manually traced regions in both humans (Allen et al., 2002; Raz et al., 2004; Raz et al., 2005) and animals (Matochik et al., 2004; Matochik et al., 2000; Tapp et al., 2004; Wisco

Send Correspondence to: Sterling C. Johnson, Geriatric Research Education and Clinical Center, Wm. S. Middleton Memorial Veterans Hospital, 2500 Overlook Terrace (11G), Madison, WI 53705, Phone 608-256-1901, Fax 608-280-7165, scj@medicine.wisc.edu.

et al., 2008) to look at structural brain changes in tissue volume. Though valued for their careful analysis, region of interest analyses are tedious to complete on large numbers of participants, and can be limited in the number of regions that are investigated and possibly confounded by rater bias. The advent of voxel-based morphometry (VBM) and automated tissue segmentation algorithms provide an opportunity to study the entire brain or specific regions with a rater free approach (Ashburner, 2007; Ashburner and Friston, 1999, 2000, 2005; Good et al., 2001; Senjem et al., 2005). These methods are widely available and due to their ease of use, are increasingly applied in human studies of brain structure. Despite a large increase in the number VBM studies (156 publications from 1999 to 2004 compared to 402 publications from 2005 to 2007), there are dramatically fewer VBM studies in nonhuman primates due, in part, to the lack of available species specific voxel-wise methods (Alexander et al., 2008; Colman et al., 2009; Oakes et al., 2007). Recently, our laboratory published a rhesus macaque MRI atlas collection that includes tissue prior probability maps (McLaren et al., 2009) facilitating VBM analysis in software packages such as Statistical Parametric Mapping (SPM5, Wellcome Department of Imaging Neuroscience, University College London, UK) or the FMRIB Software Library (FSL, Functional MRI of the Brain Centre, University of Oxford, UK).

VBM analysis consists of segmenting structural brain images into tissue classes, normalizing the segmented images to a standard space, smoothing the images, and carrying out statistical tests at each voxel. Segmentation in SPM5 requires: (i) a priori knowledge of the probability that a given voxel will belong to a given tissue class; and (ii) a template space to normalize the segmented images. In SPM5, the segmentation and normalization are done together (Ashburner and Friston, 2005). In contrast, FSL does not depend on prior probability maps of tissue classes and segments the images prior to normalization to a template space. While both SPM and FSL have seen limited use in animal studies, VBM studies using these software in animals are likely to increase in number as a result of tool development, including the development of brain atlases for: *Macaca fascicularis* (Vincent et al., 2007), *Macaca mulatta* (McLaren et al., 2009), *Macaca nemestrina* (Black et al., 2001a), *Papio anubis* (Black et al., 1997; Black et al., 2001b; Greer et al., 2002), R2/6 mouse (Sawiak et al., 2009), and 129S1/SvImJ male mouse (Kovacevic et al., 2005). At present, only the *Macaca mulatta* and R2/6 mouse atlases also contain prior probability maps for each tissue class, facilitating the use of SPM5 for VBM studies in these species (McLaren et al., 2009; Sawiak et al., 2009).

In the rhesus macaque, Alexander and colleagues (Alexander et al., 2008) reported age-related declines in the grey matter of the bilateral dorsolateral and ventrolateral prefrontal cortex, orbitofrontal cortex, lateral fissure, and superior temporal sulcal region. Increased grey-matter volume was found in the cerebellum, left visual cortex, bilateral globus pallidus, and left parietal region. Interestingly, they did not reproduce the early findings of Matochik showing changes in the caudate or putamen (Alexander et al., 2008; Matochik et al., 2000). They attributed the conflicting results to the quality of segmentation of subcortical structures and suggested that future work should investigate the impact of tissue segmentation methods (Alexander et al., 2008).

More recently, Colman and colleagues used VBM to investigate the effects of caloric restriction on aging in the rhesus macaque brain (Colman et al., 2009). Briefly, they found aged related decreases in regions including the arcuate sulcus, lateral sulcus, and superior temporal sulcus. With respect to diet, control monkeys had significant reduced grey matter volume in the putamen and caudate bilaterally. They also reported that caloric restriction eliminated the age-related decreases of grey matter volume in the right cingulate.

With VBM studies in non-human primates emerging, it is important that widely available analytic methods be used to enable replication and standardization(Alexander et al., 2008). Thus, the focus of the present study was to investigate method-related sources of variance in

VBM studies as applied to a nonhuman primate model. The present study evaluated regional brain volume in middle-aged and elderly rhesus macaques with multiple VBM methods. Specifically, we tested the effect of the segmentation algorithm, the normalization routine, and the degree of smoothing. Additionally, we consider the issues of sample size and corrections for multiple comparisons.

2. Methodological Description

2.1 Animals

A total of 17 rhesus macaques (*Macaca mulatta*; 9 males, 8 females, mean age = 23.57 years, ± 2.81 years) underwent magnetic resonance imaging (MRI) at the University of Wisconsin – Madison. All monkeys belonged to the existing primate colony at the Wisconsin National Primate Research Center at the University of Wisconsin, Madison (WNPRC/UW), Madison, WI, USA; accredited by the Association for Assessment and Accreditation of Laboratory Animal Care. Additionally, the research protocol was approved the Research Animal Resources Center at the University of Wisconsin.

2.2 Anesthesia

During the scanning procedure, the monkeys were anesthetized with ketamine (up to 15 mg/kg [100 mg/ml], IM) or alternative anesthesia in consultation with a WNPRC veterinarian and xylazine (up to 0.6 mg/kg [20 mg/ml], IM). Occasionally, animals were re-sedated during the scan with additional ketamine HCl (7–15 mg/kg [100 mg/ml], IM or IV) with or without xylazine (0.2–0.6 mg/kg [20 mg/ml], IM or IV).

2.3 Magnetic Resonance Imaging (MRI)

Images were acquired on a General Electric 3.0 T Signa MR unit (GE Medical Systems, Milwaukee, WI, USA) using a quadrature Tx/Rx volume coil with an 18cm diameter at the Waisman Center for Brain Imaging in Madison, WI, USA. Three-dimensional coronal T1-weighted inversion recovery-prepped spoiled gradient echo (IR-prepped SPGR) images were acquired with the following parameters: repetition time = 8.772 ms; echo time = 1.876 ms; inversion time = 600 ms; flip angle = 10°; number of excitations = 2; acquisition matrix = 256×256; field of view = 160mm. 124 coronal slices with a thickness of 0.7 mm were acquired resulting in 0.625 × 0.625 × 0.7 mm voxels.

2.4 MRI Image Processing

All images were manually de-skulled and rotated and translated to match the left, posterior, inferior orientation of the 112RM-SL brain (McLaren et al., 2009; Saleem and Logothetis, 2006) before entering the segmentation procedures. After segmentation and spatial normalization, grey matter segments were smoothed with a 2mm, 4mm or 8mm FWHM Gaussian filter. Spatial normalization refers to estimating and applying an affine and/or non-linear warp to an image to bring it into a target space. In the present paper, images are spatially normalized to the 112RM-SL space (McLaren et al., 2009).

2.5.1 Segmentation using FSL—Images were segmented using the FAST algorithm in FSL3.3 (Zhang et al., 2001) which provides probability maps for grey matter, white matter, and cerebral spinal fluid. With the exception of reducing the bias correction field smoothing iterations to 75 from the default of 100, no other parameters were modified. The FAST algorithm employs an expectation-maximization algorithm that uses a mixture of Gaussians plus information from hidden markov random fields and neighbors to compute the tissue probabilities at each voxel. Notably, the FAST algorithm does not require *a priori* knowledge about tissue class locations. Following segmentation, the grey matter segments were spatially

normalized in SPM5 to grey matter priors (http://brainmap.wisc.edu/monkey.html, see -- McLaren et al., 2009); using an affine transformation with non-linear components (Ashburner and Friston, 1999). The spatially normalized probability maps were then modulated (to correct for local expansion or contraction) by multiplying by the Jacobian determinant of the spatial normalization step (Good et al., 2001).

2.5.2 Segmentation using SPM—We implemented the "unified segmentation" routine in the SPM5 framework (Ashburner and Friston, 2005). The manually de-skulled images were segmented with the "segment" function. The unified segmentation process in SPM5 uses an objective cost function that integrates: (i) the prior probabilities; (ii) a mixture of Gaussians; and (iii) a registration term (Ashburner and Friston, 2005). The rotation and translation (see section 2.4) of the images prior to the "segment" routine is necessary because of the registration term in the cost function and the use of prior probabilities. Compared to the default settings, the following parameters were changed: human tissue priors were replaced by macaque tissue priors; affine regularization was changed to "average sized template"; and sampling distance was reduced to 2. This process results in a segmented and spatially normalized image, which is subsequently modulated (to correct for local expansion or contraction) by multiplying voxel values in the segmented images by the Jacobian determinants derived from the spatial normalization (Good et al., 2001).

2.5.3 DARTEL—DARTEL stands for "Diffeomorphic Anatomical Registration using Exponentiated Lie Algebra" (Ashburner, 2007). The goal of DARTEL is to preserve the topology of the brain via constant velocity flow fields. Briefly, rigidly aligned grey and white matter segments are averaged to create an initial template for each tissue class. Rigid transformation of the FSL segments was performed by applying the rigid-body component of the spatial normalization transform to the grey matter probability maps. Rigid transformation of the SPM segments was performed by applying the rigid-body component of the normalization transform to the T1-weighted images and then segmenting the images using the segmentation parameters (e.g. mixture of Gaussians) obtained during the "unified segmentation" process. Changes from the default settings included: setting to bounding box to be −40 to 40, −61 to 35, and −20 to 45; and changing the voxel size to 0.5mm. Rigid transformations are necessary as DARTEL uses a constant velocity framework, which is sensitive to translational shifts (Ashburner, 2007). Using the initial template, flow fields are created for each individual to match their segments to the template segments, which is done simultaneously for grey and white matter. The resulting deformation is averaged to create a second template. The sequence of computing flow fields and averaging the images to create a template is repeated six times. We chose the linear bend energy as the cost function. After warping the images to the final template, the images are modulated by multiplying by the Jacobian determinant of the warp field (Ashburner, 2007; Good et al., 2001). Next, we applied an affine transformation, computed by spatially normalizing the final grey matter template to the a priori grey matter probability map (McLaren et al., 2009), to each modulated and warped image to align it 112RM-SL atlas (http://brainmap.wisc.edu/monkey.html, see -- McLaren et al., 2009).

2.6 Spatial Normalization

To determine the best spatial normalization routine, we evaluated the differences in the normalized mutual information (NMI). For both FSL and SPM segmentations, the NMI between the a priori grey matter probability map and unmodulated warped grey matter segments from each individual were computed. For DARTEL, the normalized mutual information between the final grey matter templates from DARTEL smoothed with a 1mm FWHM Gaussian filter and unmodulated warped segments from each individual were computed. The DARTEL templates were smoothed to the same extent as the a priori probability

maps (McLaren et al., 2009) to avoid biasing the results based on the smoothness of the templates. Wilcoxon matched pairs signed-rank tests were computed for the following combinations: FSL and SPM; FSL using DARTEL and SPM using DARTEL; and FSL and SPM using DARTEL compared to FSL and SPM, respectively.

2.7 Smoothing

To determine the degree of smoothing that is comparable to humans, we computed the ratio of the full-width half maximum (FWHM) of the images with and without smoothing. The FWHM of the images represents the spatial smoothness across the voxels in the image. As the spatial smoothness increases, the voxel values are more similar to each other. In the present study, the FWHM was estimated using 3dFWHMx in Analysis of Functional NeuroImaging (AFNI, Cox, 1996; Forman et al., 1995) with the input as the square root of the mean squared error of the regression models (see below). This image was used to avoid biasing the estimate with the underlying structural anatomy. We also computed the degree of smoothing in seventeen human participants (46–65 years old) processed with and without DARTEL, as above, using the square root of mean error of regression models with age, gender, and total brain volume as regressors. For humans, images were either not smoothed or smoothed with 4mm, 8mm, and 12mm FWHM Gaussian kernels.

2.8 Statistical Analyses

The relationship between grey matter volume and age was evaluated using the products of FSL segmentation and SPM segmentation routines, smoothed with each Gaussian kernel. Additionally, the relationship between age and grey matter volume was assessed using SPM5 and FSL segmentations spatially normalized with and without DARTEL and using all three smoothing kernels. Sex and total brain volume (grey matter plus white matter volume from the segmentation routines) were included as covariates in all of the regression models. Additionally, whole brain volume was regressed against age and gender.

We computed T-statistics for each model evaluating cross-sectional increases and decreases in regional brain volume with age. The T-statistic maps were displayed at an uncorrected $p < 0.005$ (T-statistic > 3.0123, 13 degrees of freedom) in at least 20 edge-connected voxels. An uncorrected threshold was chosen to allow more voxels to be detected. Additionally, results were limited to areas with a grey matter prior probability greater than 0.2 (678,850 voxels for SPM with DARTEL). To determine the optimal VBM method, we used three criteria: significance of the statistic, number of significant voxels, and biological plausibility of the finding (e.g. is the area implicated in aging? is it a registration artifact near a tissue boundary?). All coordinates are in the space of the Saleem-Logothetis atlas (Saleem and Logothetis, 2006). We report the local maxima in each cluster separated by a distance of 8mm.

2.9 Multiple Comparison Correction and Power Analyses

Multiple comparison corrections for SPM with DARTEL smoothed with a 2mm or 4mm FWHM Gaussian kernel were computed using the false discovery rate method (Genovese et al., 2002), and using AlphaSim in AFNI (Cox, 1996; Forman et al., 1995). Additionally, we computed the sample size needed to detect the same voxels in uncorrected map when controlling for the false discovery rate.

3. Results

3.1 Registration Accuracy as Measured with Normalized Mutual Information

Less than optimal registration confounds the statistical results as differences might be due to misregistration as opposed to true morphological differences (Bookstein, 2001). We found that

registration accuracy was higher with SPM compared to FSL and higher with DARTEL than without DARTEL. The mean of the normalized mutual information (NMI) of the template grey matter image (*a priori* grey matter probability map or DARTEL grey matter template) and the normalized and segmented images are (mean±SD): 1.221±.008, 1.179±.013, 1.246±.006, 1.244±.011 for "unified segmentation" in SPM, segmentation using FSL, "unified segmentation" in SPM normalization with DARTEL, and segmentation using FSL and normalization with DARTEL, respectively. The NMI was significantly higher for SPM without DARTEL compared to FSL without DARTEL ($p=1.53\times10^{-5}$) using a Wilcoxon matched pairs signed-rank test. This might be explained by the use of priors, which would increase the mutual information of the images and the template. However, one should still consider that the lower NMI might indicate that the results might be more likely due to registration difficulties with FSL segments as compared to SPM segments. For example, figure 1 (cyan arrows) illustrates several regions that were not well segmented by FSL, which would both hinder the registration and decrease the NMI.

The NMI for SPM with DARTEL and FSL with DARTEL was significantly greater than the NMI for SPM without DARTEL ($P=1.53\times10^{-5}$) and FSL without DARTEL ($P=1.53\times10^{-5}$), respectively, as assessed using Wilcoxon matched- pairs signed-rank tests. NMI of SPM segmentation and normalization with DARTEL was not significantly different from the FSL segmentation and normalization with DARTEL ($p=0.279$) using the Wilcoxon matched pairs signed-rank test. While the NMI indicates that both FSL and SPM inputs result in a similar alignment; inspecting the images revealed a few differences. Figure 1 illustrates the results of a monkey processed with FSL and SPM. FSL segmentations tended to be more rigid in the segmentation results evidenced by a sharper transition between grey and white matter. Additionally, in areas where there is less contrast in the T1-weighted scan, FSL has lower probabilities (cyan arrows). As seen in figure 1, processing the images with DARTEL did not ameliorate these differences.

Interestingly, the NMI from FSL segments for both the low dimensional non-linear normalization and DARTEL were negatively correlated with age after controlling for gender ($p=0.0399$ and $p=0.0258$, respectively).

3.2 Smoothing

The effect of smoothing is illustrated in figure 1. When the segments are smoothed with an 8mm FWHM Gaussian filter, there is a substantial loss in anatomical information. From the least to most smooth, the FWHM increases by a factor of 1.92, 4.01, and 6.9 for 2mm, 4mm, and 8mm filters, respectively with SPM. When DARTEL is used with the SPM segments, FWHM increases by factors of 1.66, 2.44, and 4.25. With FSL alone and FSL with DARTEL the FWHM increases by factors of 1.98, 4.10, and 7.40 and 1.56, 2.40, and 4.18, respectively.

In humans, the increase in FWHM with and without using DARTEL for normalization did not exceed 1.81 even when smoothed with a 12mm FWHM Gaussian kernel. Thus, in order to achieve comparable smoothness to that in humans, 2mm to 4mm kernels should be used to smooth data.

3.3 Effect of Age (Global Analyses)

We found no relationship between global brain volume and age for any method.

3.4 Effect of Age (VBM Analyses)

3.4.1 FSL—FSL segments normalized without DARTEL had a smoothness of 1.39mm FWHM. For segments smoothed with a 2mm, 4mm, and 8mm FWHM Gaussian kernel, the

smoothness of the smoothed segments was 2.75mm FWHM, 5.71mm FWHM, and 10.30mm FWHM, respectively.

Smoothed using a 2mm FWHM Gaussian kernel: Grey matter volume decreases were observed in eighty-two clusters (ranging in size from 2.50mm^3 to 69.625mm^3) with a maximum t-statistic of 7.55 (Figure 2 top row, Table S1). Clusters were located in regions including: primary visual cortex, secondary visual cortex, higher visual areas (e.g. V3v, V4, 7a), the superior temporal sulcus, agranular frontal areas, the caudate, hippocampus and entorhinal cortex, somatosensory cortices, the cerebellum and white matter within several gyri. A total volume of 783.75mm^3 showed age-related decreases.

Increases in grey matter volume with age were found in 7 clusters (ranging in size from in 2.875mm^3 to 12.625mm^3): primary visual cortex, secondary visual cortex, area 7m, the lunate sulcus, temporal pole, cerebellum, and optic tract (Figure 2 top row, Table S1). The total volume for these clusters is 33.00mm^3.

Smoothed using a 4mm FWHM Gaussian kernel: Grey matter volume decreases were observed in forty-three clusters (ranging in size from 2.75mm^3 to 454.37mm^3) with a maximum t-statistics of 5.84. A total grey matter volume of 1892.50mm^3 showed age-related decreases and included regions such as: primary visual cortex, secondary visual cortex, higher visual areas (e.g. V3d and V4), agranular frontal areas, the caudate, somatosensory cortices, the cerebellum, arcuate sulcus and posterior cingulate cortex (Figure 2 middle row, Table S2). There were no voxels that passed the threshold for age-related volume increases.

Smoothed using an 8mm FWHM Gaussian kernel: Grey matter volume decreases were observed in ten clusters (ranging in size from 3.625 mm^3 to 3470.25 mm^3) with a maximum t-statistic of 5.80 (Figure 2 bottom row, Table S3). The peak coordinates from these clusters were located in regions that included: primary visual cortex, occipital cortex (V4) through the posterior cingulate cortex to primary somatosensory cortex, the caudate, secondary somatosensory cortex and the cerebellum. A total volume of 3780.63mm^3 showed age-related decreases. There were no voxels that passed the threshold for age-related increases in brain volume.

3.4.2 SPM—SPM segments normalized without DARTEL had a smoothness of 1.23mm FWHM. For segments smoothed with a 2mm, 4mm, and 8mm FWHM Gaussian kernel, the smoothness of the smoothed segments was 2.37mm FWHM, 4.95mm FWHM, and 8.54mm FWHM, respectively.

Smoothed using an 2mm FWHM Gaussian kernel: Age associated grey matter volume decreases were found in sixty-one clusters (ranging in size from 2.5mm^3 to 61.25mm^3) with a peak T-statistic of 9.65. A total of 771.875mm^3 of grey matter showed age-related decreases. Clusters were found in regions that included: Clusters were located in regions including: primary visual cortex, secondary visual cortex, higher visual areas (e.g. V3A, V4, 7a), the superior temporal sulcus, agranular frontal areas, the caudate, hippocampus, somatosensory cortices, the cerebellum, posterior cingulate cortex and the superior temporal gyrus (Figure 3 top row, Table S4).

Eleven clusters showed age associated grey matter increases (ranging in size from in 3.375mm^3 to 14.625mm^3) including: primary visual cortex, area 7m area TEO, prefrontal cortex (area 46d), the putamen and cerebellum (Figure 3 top row, Table S4). A total volume of 100.50mm^3 showed age-related increases.

Smoothed using an 4mm FWHM Gaussian kernel: Age associated grey matter volume decreases were found in twenty-seven clusters (ranging in size from 3.5mm^3 to 116.125mm^3) with a peak T-statistic of 5.5. A total of 637.125mm^3 of grey matter showed age associated decreases. Clusters were located in regions including: primary visual cortex, secondary visual cortex, the superior temporal sulcus, caudate, entorhinal cortex, somatosensory cortices, the cerebellum and superior temporal gyrus (Figure 3 middle row, Table S5).

One cluster (6mm^3 in size) in primary visual cortex showed an age associated increase in grey matter volume (Figure 3 middle row, Table S5).

Smoothed using an 8mm FWHM Gaussian kernel: Age associated grey matter volume decreases were found in two regions. One cluster (67mm^3) with a peak T-statistic of 3.69 was in the superior temporal gyrus and another cluster (3.25mm^3) was found in the posterior cingulate cortex (Figure 3 bottom row, Table S6). No voxels showing age associated increases in grey matter volume passed the threshold.

3.4.3 DARTEL and FSL—FSL segments normalized with DARTEL had a smoothness of 2.15mm FWHM. For segments smoothed with a 2mm, 4mm, and 8mm FWHM Gaussian kernel, the smoothness of the smoothed segments was 3.36mm FWHM, 5.15mm FWHM, and 8.97mm FWHM, respectively.

Smoothed using a 2mm FWHM Gaussian kernel: Grey matter decreases with age were found in fifty-one clusters (ranging in size from 2.75mm^3 to 231.875mm^3) with a peak T-statistic of 7.79. A total of 1534.75mm^3 of grey matter volume showed age associated decreases. Clusters were located in regions including: primary visual cortex, secondary visual cortex, higher visual areas (e.g. V3A and V4), the superior temporal sulcus, agranular frontal areas, the caudate, hippocampus, posterior cingulate cortex, somatosensory cortices, the cerebellum and arcuate sulcus (Figure 4 top row, Table S7).

Seven clusters showed increases in grey matter volume with age (ranging in size from 3.25mm^3 to 30.25mm^3). Clusters were found in secondary visual cortex, the corpus callosum, lateral sulcus, area TFO, the cerebellum and somatosensory area 5 (Figure 4 top row, Table S7). A total volume of 77.00mm^3 showed age-related increases.

Smoothed using a 4mm FWHM Gaussian kernel: Grey matter volume decreases with age were found in twenty-one clusters (ranging in size from 2.625mm^3 to 352.125mm^3) with a peak T-statistic of 6.72. A total of 2238.625mm^3 of grey matter showed age associated decreases. The clusters were found in regions that included: primary visual cortex, secondary visual cortex, agranular frontal area F1, the caudate, posterior cingulate cortex, somatosensory cortices and the arucate sulcus (Figure 4 middle row, Table S8).

Age associated increases in grey matter volume with age were found in one cluster (11.875mm^3) located in the cerebellum (Figure 4 middle row, Table S8).

Smoothed using an 8mm FWHM Gaussian kernel: Eight clusters showed decreases in grey matter volume with age. The clusters ranged in size from 52.875mm^3 to 1281.375mm^3 and were found in regions that included: primary visual cortex, secondary visual cortex, the caudate, retrosplenial and posterior cingulate cortex, primary somatosensory cortex and the arcuate sulcus (Figure 4 bottom row, Table S9). A total of 4035.25mm^3 of grey matter showed age associated decreases. No age associated increases in grey matter volume passed threshold.

3.4.4 DARTEL and SPM—SPM segments normalized with DARTEL had a smoothness of 1.82mm FWHM. For segments smoothed with a 2mm, 4mm, and 8mm FWHM Gaussian kernel, the smoothness of the smoothed segments was 3.02mm FWHM, 4.43mm FWHM, and 7.71mm FWHM, respectively.

Smoothed using a 2mm FWHM Gaussian kernel: Grey matter volume decreases with age were found in twenty-two clusters (ranging in size from 2.75mm^3 to 44.25mm^3) with a peak T-statistic of 5.74. Clusters were found in regions that included: the occipital lobe (V2 and V4), superior temporal sulcus, caudate, hippocampus, retrosplenial and posterior cingulate cortex, somatosensory cortex, the cerebellum, arcuate sulcus and insula (Figure 5 top row, Table S10). A total of 282.25mm^3 of grey matter showed age associated decreases.

Eleven clusters (ranging in size from 2.5mm^3 to 31.75mm^3) showed age associated increases in grey matter volume. Clusters were found in regions that included: primary visual cortex, the cerebellum, posterior cingulate cortex, somatosensory area 5, agranular frontal area F2 and retrosplenial cortex (Figure 5 top row, Table S10). A total volume of 113.38mm^3 showed age-related increases.

Smoothed using a 4mm FWHM Gaussian kernel: Age associated decreases in grey matter volume were found in six clusters (ranging in size from 7.375mm^3 to 106.13mm^3) with a peak T-statistic of 4.62. Clusters were located in secondary visual cortex, the caudate, retrosplenial and posterior cingulate cortex and the arcuate sulcus (Figure 5 middle row, Table S11). A total 260.25mm^3 of grey matter showed age associated decreases in volume.

Increases in grey matter volume with age were found in the posterior cingulate cortex (3.38mm^3)and cerebellum (30.38mm^3, Figure 5 middle row, Table S11).

Smoothed using an 8mm FWHM Gaussian kernel: Decreases in grey matter volume with age were found bilaterally in retroplenial and posterior cingulated cortex (Figure 5 bottom row, Table S12). No age associated increases passed the threshold.

3.5 Multiple Comparison Corrections and Power Analysis

When the statistical map from SPM with DARTEL smoothed with a 2mm FWHM Gaussian kernel for age-related decreases in regional grey matter volume was corrected for multiple comparisons controlling for the false discovery rate (FDR) of 0.05 there were no significant voxels. In order for any voxels to survive, the most significant T-statistic would need to have been greater than 10.1736. We computed the necessary sample size to achieve the same map with FDR correction applied. At 80% and 90% power, respectively, the sample size would need to be 37 and 45 animals to detect the same voxels controlling for the FDR at 0.05 based on the current effect sizes. If the FDR is not controlled, but voxels with an effect size of .6980 (Cohen's f^2), which corresponds to our liberal threshold of $p<0.005$, are to be detected at an alpha=0.0001, the sample size needs to be 39 and 47 animals for 80% and 90% power, respectively.

When the statistical map of age-related declines produced using SPM and DARTEL (smoothed at 4mm) was corrected for multiple comparisons using FDR of 0.05, no voxels passed the threshold. In order for any voxels to survive, the most significant T-statistic would need to have been greater than 10.1736. Using a mask created by thresholding the prior probability at 0.2 (678,850 voxels), we computed the necessary sample size to achieve the same map controlling for the FDR at a level of 0.05. The results were the same as above.

We also tried to correct for multiple comparisons using an extent threshold determined from AlphaSim (Cox, 1996; Forman et al., 1995). Neither the SPM with DARTEL smoothed with

a 2mm or 4mm kernel had clusters that exceeded the threshold. The minimum cluster sizes for a voxel threshold of $p<0.005$ were 471 voxels (58.875 mm^3) and 1159 voxels (144.875 mm^3) for data smoothed with a 2mm and 4mm kernel, respectively. If the voxel threshold is reduced to $p<0.0001$, then the extent thresholds would drop to 78 voxels (9.75 mm^3) and 171 voxels (21.375 mm^3). As noted above, all voxels in the uncorrected maps could be detected at this voxel threshold with 90% power with a sample size of 47 individuals. Additionally, with the smaller cluster extent, several clusters would be significant with the correction for multiple comparisons.

4. Discussion

Several studies support age-related volume change in both humans and non-humans. While some studies show age-related changes in primary cortices (Peters et al., 2001; Peters et al., 1996; Salat et al., 2004), the majority of studies show preferential effects of aging in association areas (Alexander et al., 2008; Colman et al., 2009; Good et al., 2001; Matochik et al., 2000; Raz et al., 1997; Raz et al., 2005; Sowell et al., 2004b; Tapp et al., 2006; Tapp et al., 2004). Importantly, Andersen and colleagues have shown that changes in rhesus macaques are similar to those in humans (Andersen et al., 1999), thus allowing us to use both species to interpret which methods produced plausible results in the present analysis.

4.1. Effect of Using DARTEL

While it could be argued that affine registration techniques should be sufficient for small animals and perhaps some non-human primates that have smoother cortices than humans (Black et al., 2001a; Black et al., 2001b; McLaren, 2008); any suboptimal registration influences our interpretation of the results since statistical effects may be driven by poor registration instead of morphological differences (Bookstein, 2001). Consequently, DARTEL may be a better alternative for VBM studies in animals as well as humans given its superior normalization ability across individuals.

In addition to the current results that show an increase in the normalized mutual information when using DARTEL to coregister scans in macaques, DARTEL has also been shown to increase the registration accuracy between human participants (Ashburner, 2007; Klein et al., 2009). Surface-based analyses, when compared to affine or low non-linear normalization procedures, show improved coregistration (Fischl et al., 2007; Van Essen, 2005); this benefit potentially allowed Salat et al. to reveal thinning in primary cortices (Salat et al., 2004). If DARTEL can approach the surface-based methods, then changes in primary cortices as well as association areas would not be unexpected.

In using DARTEL, we can be more confident that the effects are morphological rather than errors in registering participants to a target (Bookstein, 2001). The smoothing kernel with DARTEL should be smaller than with other normalization algorithms as one goal of smoothing with a larger kernel is to reduce variability between individuals

4.2 Effect of the Smoothing Kernel

The effects of smoothing were predictable. As the kernel increased in size, the detection of larger clusters was increased at the expense of smoothing smaller clusters under the noise floor. Human morphometry studies typically use smoothing kernels ranging in size from 6 to 12 millimeters. The only VBM study in a non-human species of similar size to the rhesus macaques was in a canine study of aging (Tapp et al., 2006). In that study, the smoothing kernel was 2mm FWHM. In the present study, 2mm, 4mm, and 8mm kernels were evaluated. Based on the number of clusters, biological plausibility of the results, and relative increase in smoothness

of the data compared to humans, we concluded that 4mm FWHM should be the upper limit of the smoothing kernel in rhesus macaques.

4.3 FSL versus SPM

Voxel-based morphometry studies rely on the assumption that the segmentation is accurate. Neither smoothing nor using DARTEL ameliorates the effects of poor segmentation. Thus, the comparison between FSL and SPM is a comparison of the segmentation procedures.

When using DARTEL, and a smaller smoothing kernel, both the FSL and SPM analyses produced similar and anatomically plausible brains such as the caudate (Matochik et al., 2000) and agranular frontal area F2 (Alexander et al., 2008; Colman et al., 2009). However, several differences between FSL and SPM segmentation were also found. Normalization accuracy was higher with SPM and was not negatively correlated with age. Both decreased accuracy and age correlations when using segments from FSL may increase the number and size of clusters. Thus, the inferences might be the result of these problems and not due to volume changes (Bookstein, 2001). For example, widening between hemispheres can be seen on both the FSL and SPM segments in the medial occipital lobe; however, only the analyses using the FSL produced segments showing correlations between medial occipital brain volume and age. It is possible that this difference is the result of misregistration and not a change in brain morphometry. One possibility for the misregistration is that the constant velocity framework of DARTEL might be problematic for the rigid segmentations (sharper edges of grey matter) produced by FSL, especially in regions where there is less identifiable grey matter (21). Further investigation into using a constant velocity framework with varying image quality and types (e.g. segmentation routines) is necessary to fully elucidate the source of the registration difficulty. Furthermore, FSL without DARTEL detected numerous clusters that were isolated to white matter (e.g. white matter in the premotor cortex). While FSL segmentation produced larger clusters with more robust t-statistics suggesting, concerns over their biological plausibility of some clusters due to issues of segmentation quality and the accuracy of registration lead to recommending using SPM for non-human primates over FSL.

4.4 Multiple Comparison Corrections

Multiple-comparison correction procedures that correct inferences at the voxel level penalize studies that have higher number of voxels. As the number of voxels increase, the number of individuals in the study needs to increase to detect the same area. While there are several possible solutions, all of them have their drawbacks.

Decreasing the resolution of the image will result in fewer voxels and, assuming the statistics are the same, potentially reveal more regions that are truly significant. However, the cortical ribbon in rhesus macaques is approximately 1.7 to 2.5mm thick (Hinds et al., 2008; Juchem et al., 2007; Mountcastle, 1998), whereas in humans it is usually 3–6mm thick (Sowell et al., 2004a; Sowell et al., 2004b). As the voxel size increases, the ability to detect subtle changes in the macaque will be decreased.

With large sample sizes, one is more likely to detect significant effects even with voxel-wise corrections. To achieve 90% power for FDR correction that would detect the same voxels as the present study, the sample size would need to be 45 individuals. This number is likely conservative as the voxels considered had to be in clusters of at least 20 voxels. Future studies with larger samples should investigate proposed methods of correcting for the false discovery rate at the cluster level as this implies that there are voxels that also meet the false discovery rate correction (Benjamini and Heller, 2007; Chen et al., 2008; Chumbley and Friston, 2009).

Using a liberal threshold ($p<0.005$) with an extent threshold of 1159 voxels (144.875 mm^3), as determined using AlphaSim as the extent necessary to correct for multiple comparisons, for data smoothed with a 4mm FWHM Gaussian kernel is problematic as the median region volume of major cortical and subcortical regions identified from the digital Paxinos Atlas (Bezgin et al., 2009; Paxinos et al., 2008) is 120.12 mm^3 (Moirano, J. and Converse, A.K., personal communication). Given that regional brain volume changes are likely to occur in only parts of any region, the cluster size must be significantly smaller than the region. Thus, future studies will need more robust results to reduce the cluster extent threshold.

An alternative to voxel-wise procedures is multivariate tests. Alexander et al. recently demonstrated the feasibility of multivariate testing in rhesus macaques and required a much smaller sample (Alexander et al., 2008). There are several caveats for interpreting the differences between their study and ours: (i) their age range was coded into young and old animals rather than as a continuous variable; (ii) the difference between their old and young animals was larger than the age range studied in the present sample; and (iii) small regions that have morphometry changes not consistent with the main patterns might not be detected. While some results between the two studies are consistent, for example the results in agranular frontal area F2; while other results were not, such as our findings of decrease in the caudate -- which is consistent with other studies (Matochik et al., 2000; Wisco et al., 2007). Nevertheless, the multivariate approach presents a very promising alternative to voxel-based morphometry that provides complementary and unique information on brain aging (Alexander et al., 2008).

4.5 Limitations

The major limitation to this approach is that there is no ground truth to which the segmentation methods can be compared. Thus, conclusions regarding the relative superiority of any approach are tentative and may be affected greatly by modifying the parameters of each approach. The results of the present study are limited to the specific parameters used. In order to use SPM, one must first rotate and set the origin of each brain to match that of the template. Incomplete or less than optimal segmentation may result without performing this step since the cost function of the algorithm has a penalty term for translations and rotations. Furthermore, optimization of segmentation in FSL by changing the algorithm or parameters may change the results. The chosen parameters for the segmentation and normalization routines are the default parameters of each software package, SPM and FSL, which have been optimized for human studies. Although a major implication of the present findings is that VBM can be adapted for NHP models, the general methodology of VBM was developed for application to the human brain, and other parameters, beyond those we tested, may be necessary to investigate to obtain an optimized approach to NHP VBM (see section 4.6 for an example).

As has been the case in previous studies, it is possible that age can interact with the segmentation routine, due to imaging artifacts caused by iron and calcium deposition in addition to larger sulci and fissures (Davatzikos and Resnick, 2002; Ogg and Steen, 1998). Although these artifacts can complicate the interpretations of the physiological basis of the results, they do not preclude the conclusions that can be draw with regard to age-related differences. For example, we observed an effect of age on volume in the visual cortex. Regardless of whether this is a true effect of age on grey matter volume or an effect of age on iron deposition, our technique still identified a relationship between age and the properties of the tissue. Thus, results on volume change may need to be interpreted with caution as they may be due to changes in the tissue properties and related changes to T1 signal with age (Ogg and Steen, 1998). Either way, significant results, at least with DARTEL, are more likely to reflect changes in the brain as opposed to misregistration.

The present study did not explicitly test the difference in regression lines between studies for several reasons. First, the goal of the study is to identify which method is optimal for detecting

aging effects. Second, since all four processing streams use different normalization parameters, voxels from the original image are shifted to different locations with each processing stream. This precludes directly comparing the slopes between models.

Due to the small sample size, results were reported with a liberal threshold. Future studies will be needed that include a larger age range to better map the complete course of age-related change in macaque morphology. In a mixed sample of calorie restricted rhesus macaques and rhesus macaques fed *ad libitum*, the age-related findings in the agranular frontal areas and arcuate sulcus are replicated (Colman et al., 2009).

4.6 Alternatives

Future VBM studies in animals might want to consider several alternative approaches that were not evaluated in this study. First, in human imaging there are still questions regarding whether or not VBM studies should use modulated or unmodulated images in their statistical analyses (Eckert et al., 2006). Secondly, the use of hidden markov random fields (HMRF) in the FSL segmentation, but not SPM raises the question: whether the lack of priors or the use of HMRF mediated the results? Gaser and colleagues provide a toolbox (VBM5.1, http://dbm.neuro.uni-jena.de/vbm/) for SPM that allows the use of priors and HMRF. Future studies should investigate whether or not the use of priors and HMRF improves the segmentation in SPM for animals.

Salat and colleagues have used surface-based approaches to measure cortical thickness and align participants based on the curvature pattern in the brain (Fischl and Dale, 2000; Fischl et al., 1999; Salat et al., 2004). Similar studies in non-humans would yield valuable results and should be the aim of future studies. Surface-based analyses may be done in CARET, which already contains surface templates for the rhesus macaque and the cynomolgus monkey (Van Essen, 2004; Van Essen and Dierker, 2007; Van Essen et al., 2001a; Van Essen et al., 2001b; Vincent et al., 2007). In addition to non-human primate atlases, CARET also has several human atlases that facilitate comparisons between primate species (Van Essen, 2005; Van Essen and Dierker, 2007).

5. Concluding Remarks

The results of the present study suggest that methods of data analysis can affect the final results of VBM studies in rhesus macaque. Guidelines for data analysis have been provided for human VBM studies (Ridgway et al., 2008), but similar guidelines are currently lacking for the analysis of non-human primate brains. As demonstrated here, segmentation, smoothing and normalization routines have a definite impact on the data and the statistical results.

It is important to recognize the limitations of any technique (Bookstein, 2001; Ogg and Steen, 1998; Ridgway et al., 2008). Specifically, researchers should carefully consider what a decrease or increase in local grey matter represents based on the methods employed. Our results would suggest that, at least in our sample of rhesus macaques and with the specific parameters used here, using the SPM segmentation algorithm with DARTEL produces the most robust and plausible results. Additionally, our results suggest that the optimal smoothing kernel is probably between 2mm to 4mm. Finally, despite the limitations of any method, our results and those of others clearly demonstrate that software and methods developed for human imaging studies can be implemented in animal studies (Alexander et al., 2008; Colman et al., 2009; Oakes et al., 2007; Tapp et al., 2006).

Acknowledgments

This study was supported in part by the National Institutes of Health RR000167, AG11915, AG000213, and GM007507. The study was also supported with resources and use of facilities at the William S. Middleton Memorial Veterans Hospital, Madison, WI, USA. The assistance of Brent W. Thiel, Michele E. Fitzgerald, Ron Fisher, Scott T. Baum, Josh Smith, Ricki J. Colman, Ph.D., Andy. A. Alexander, Ph.D., and the Waisman Center for Brain Imaging are greatly appreciated. GRECC Manuscript Number: 2009-5.

References

Alexander GE, Chen K, Aschenbrenner M, Merkley TL, Santerre-Lemmon LE, Shamy JL, Skaggs WE, Buonocore MH, Rapp PR, Barnes CA. Age-related regional network of magnetic resonance imaging gray matter in the rhesus macaque. J Neurosci 2008;28:2710–2718. [PubMed: 18337400]

Allen JS, Damasio H, Grabowski TJ. Normal neuroanatomical variation in the human brain: an MRI-volumetric study. Am J Phys Anthropol 2002;118:341–358. [PubMed: 12124914]

Andersen AH, Zhang Z, Zhang M, Gash DM, Avison MJ. Age-associated changes in rhesus CNS composition identified by MRI. Brain Res 1999;829:90–98. [PubMed: 10350533]

Ashburner J. A fast diffeomorphic image registration algorithm. Neuroimage 2007;38:95–113. [PubMed: 17761438]

Ashburner J, Friston KJ. Nonlinear spatial normalization using basis functions. Hum Brain Mapp 1999;7:254–266. [PubMed: 10408769]

Ashburner J, Friston KJ. Voxel-based morphometry--the methods. Neuroimage 2000;11:805–821. [PubMed: 10860804]

Ashburner J, Friston KJ. Unified segmentation. Neuroimage 2005;26:839–851. [PubMed: 15955494]

Benjamini Y, Heller R. False Discovery Rates for Spatial Signals. Journal of the American Statistical Association 2007;102:1272–1281.

Beyer MK, Larsen JP, Aarsland D. Gray matter atrophy in Parkinson disease with dementia and dementia with Lewy bodies. Neurology 2007;69:747–754. [PubMed: 17709706]

Bezgin G, Reid AT, Schubert D, Kotter R. Matching spatial with ontological brain regions using java tools for visualization, database access, and integrated data analysis. Neuroinformatics 2009;7:7–22. [PubMed: 19145492]

Black KJ, Gado MH, Videen TO, Perlmutter JS. Baboon basal ganglia stereotaxy using internal MRI landmarks: validation and application to PET imaging. J Comput Assist Tomogr 1997;21:881–886. [PubMed: 9386276]

Black KJ, Koller JM, Snyder AZ, Perlmutter JS. Template images for nonhuman primate neuroimaging: 2. Macaque. Neuroimage 2001a;14:744–748. [PubMed: 11506546]

Black KJ, Snyder AZ, Koller JM, Gado MH, Perlmutter JS. Template images for nonhuman primate neuroimaging: 1. Baboon. Neuroimage 2001b;14:736–743. [PubMed: 11506545]

Bookstein FL. “Voxel-based morphometry” should not be used with imperfectly registered images. Neuroimage 2001;14:1454–1462. [PubMed: 11707101]

Brickman AM, Habeck C, Ramos MA, Scarmeas N, Stern Y. A forward application of age associated gray and white matter networks. Hum Brain Mapp. 2007a

Brickman AM, Habeck C, Zarahn E, Flynn J, Stern Y. Structural MRI covariance patterns associated with normal aging and neuropsychological functioning. Neurobiol Aging 2007b;28:284–295. [PubMed: 16469419]

Ceccarelli A, Rocca MA, Pagani E, Colombo B, Martinelli V, Comi G, Filippi M. A voxel-based morphometry study of grey matter loss in MS patients with different clinical phenotypes. Neuroimage. 2008

Chen S, Wang C, Eberly LE, Caffo BS, Schwartz BS. Adaptive control of the false discovery rate in voxel-based morphometry. Hum Brain Mapp. 2008

Chetelat G, Fouquet M, Kalpouzos G, Denghien I, De la Sayette V, Viader F, Mezenge F, Landeau B, Baron JC, Eustache F, Desgranges B. Three-dimensional surface mapping of hippocampal atrophy progression from MCI to AD and over normal aging as assessed using voxel-based morphometry. Neuropsychologia 2008;46:1721–1731. [PubMed: 18289618]

Chumbley JR, Friston KJ. False discovery rate revisited: FDR and topological inference using Gaussian random fields. Neuroimage 2009;44:62–70. [PubMed: 18603449]

Colman RJ, Anderson RM, Johnson SC, Kastman EK, Kosmatka KJ, Beasley TM, Allison DB, Cruzen C, Simmons HA, Kemnitz JW, Weindruch R. Caloric restriction delays disease onset and mortality in rhesus monkeys. Science 2009;325:201–204. [PubMed: 19590001]

Cox RW. AFNI: software for analysis and visualization of functional magnetic resonance neuroimages. Comput Biomed Res 1996;29:162–173. [PubMed: 8812068]

Davatzikos C, Resnick SM. Degenerative age changes in white matter connectivity visualized in vivo using magnetic resonance imaging. Cereb Cortex 2002;12:767–771. [PubMed: 12050088]

Eckert MA, Tenforde A, Galaburda AM, Bellugi U, Korenberg JR, Mills D, Reiss AL. To modulate or not to modulate: differing results in uniquely shaped Williams syndrome brains. Neuroimage 2006;32:1001–1007. [PubMed: 16806978]

Fischl B, Dale AM. Measuring the thickness of the human cerebral cortex from magnetic resonance images. Proc Natl Acad Sci U S A 2000;97:11050–11055. [PubMed: 10984517]

Fischl B, Rajendran N, Busa E, Augustinack J, Hinds O, Yeo BT, Mohlberg H, Amunts K, Zilles K. Cortical Folding Patterns and Predicting Cytoarchitecture. Cereb Cortex. 2007

Fischl B, Sereno MI, Tootell RB, Dale AM. High-resolution intersubject averaging and a coordinate system for the cortical surface. Hum Brain Mapp 1999;8:272–284. [PubMed: 10619420]

Forman SD, Cohen JD, Fitzgerald M, Eddy WF, Mintun MA, Noll DC. Improved assessment of significant activation in functional magnetic resonance imaging (fMRI): use of a cluster-size threshold. Magn Reson Med 1995;33:636–647. [PubMed: 7596267]

Genovese CR, Lazar NA, Nichols T. Thresholding of statistical maps in functional neuroimaging using the false discovery rate. Neuroimage 2002;15:870–878. [PubMed: 11906227]

Giorgio A, Watkins KE, Douaud G, James AC, James S, De Stefano N, Matthews PM, Smith SM, Johansen-Berg H. Changes in white matter microstructure during adolescence. Neuroimage 2008;39:52–61. [PubMed: 17919933]

Good CD, Johnsrude IS, Ashburner J, Henson RN, Friston KJ, Frackowiak RS. A voxel-based morphometric study of ageing in 465 normal adult human brains. Neuroimage 2001;14:21–36. [PubMed: 11525331]

Greer PJ, Villemagne VL, Ruszkiewicz J, Graves AK, Meltzer CC, Mathis CA, Price JC. MR atlas of the baboon brain for functional neuroimaging. Brain Res Bull 2002;58:429–438. [PubMed: 12183022]

Hamalainen A, Grau-Olivares M, Tervo S, Niskanen E, Pennanen C, Huuskonen J, Kivipelto M, Hanninen T, Tapiola M, Vanhanen M, Hallikainen M, Helkala EL, Nissinen A, Vanninen RL, Soininen H. Apolipoprotein E epsilon 4 allele is associated with increased atrophy in progressive mild cognitive impairment: a voxel-based morphometric study. Neurodegener Dis 2008;5:186–189. [PubMed: 18322386]

Hinds O, Polimeni JR, Rajendran N, Balasubramanian M, Wald LL, Augustinack JC, Wiggins G, Rosas HD, Fischl B, Schwartz EL. The intrinsic shape of human and macaque primary visual cortex. Cereb Cortex 2008;18:2586–2595. [PubMed: 18308709]

Honea RA, Meyer-Lindenberg A, Hobbs KB, Pezawas L, Mattay VS, Egan MF, Verchinski B, Passingham RE, Weinberger DR, Callicott JH. Is gray matter volume an intermediate phenotype for schizophrenia? A voxel-based morphometry study of patients with schizophrenia and their healthy siblings. Biol Psychiatry 2008;63:465–474. [PubMed: 17689500]

Juchem C, Logothetis NK, Pfeuffer J. 1H-MRS of the macaque monkey primary visual cortex at 7 T: strategies and pitfalls of shimming at the brain surface. Magn Reson Imaging 2007;25:902–912. [PubMed: 17467220]

Kalpouzos G, Chetelat G, Baron JC, Landeau B, Mevel K, Godeau C, Barre L, Constans JM, Viader F, Eustache F, Desgranges B. Voxel-based mapping of brain gray matter volume and glucose metabolism profiles in normal aging. Neurobiol Aging. 2007

Klein A, Andersson J, Ardekani BA, Ashburner J, Avants B, Chiang MC, Christensen GE, Collins DL, Gee J, Hellier P, Song JH, Jenkinson M, Lepage C, Rueckert D, Thompson P, Vercauteren T, Woods RP, Mann JJ, Parsey RV. Evaluation of 14 nonlinear deformation algorithms applied to human brain MRI registration. Neuroimage. 2009

Kovacevic N, Henderson JT, Chan E, Lifshitz N, Bishop J, Evans AC, Henkelman RM, Chen XJ. A three-dimensional MRI atlas of the mouse brain with estimates of the average and variability. Cereb Cortex 2005;15:639–645. [PubMed: 15342433]

Matochik JA, Chefer SI, Lane MA, Roth GS, Mattison JA, London ED, Ingram DK. Age-related decline in striatal volume in rhesus monkeys: assessment of long-term calorie restriction. Neurobiol Aging 2004;25:193–200. [PubMed: 14749137]

Matochik JA, Chefer SI, Lane MA, Woolf RI, Morris ED, Ingram DK, Roth GS, London ED. Age-related decline in striatal volume in monkeys as measured by magnetic resonance imaging. Neurobiol Aging 2000;21:591–598. [PubMed: 10924777]

McLaren DG, Kosmatka KJ, Oakes TR, Kroenke CD, Kohama SG, Matochik JA, Ingram DK, Johnson SC. A population-average MRI-based atlas collection of the rhesus macaque. Neuroimage 2009;45:52–59. [PubMed: 19059346]

McLaren, ea. A Population-Average MRI-Based Atlas Collection of the Rhesus Macaque. Neuroimage. 2008

Meisenzahl EM, Koutsouleris N, Gaser C, Bottlender R, Schmitt GJ, McGuire P, Decker P, Burgermeister B, Born C, Reiser M, Moller HJ. Structural brain alterations in subjects at high-risk of psychosis: A voxel-based morphometric study. Schizophr Res. 2008

Mountcastle, VB. Perceptual Neuroscience: The Cerebral Cortex. 1. Harvard University Press; 1998.

Oakes TR, Fox AS, Johnstone T, Chung MK, Kalin N, Davidson RJ. Integrating VBM into the General Linear Model with voxelwise anatomical covariates. Neuroimage 2007;34:500–508. [PubMed: 17113790]

Ogg RJ, Steen RG. Age-related changes in brain T1 are correlated with iron concentration. Magn Reson Med 1998;40:749–753. [PubMed: 9797159]

Paxinos, G.; Huang, X.; Petrides, M.; Toga, AW. The Rhesus Monkey Brain in Stereotaxic Coordinates. 2. Academic Press; 2008.

Peters A, Moss MB, Sethares C. The effects of aging on layer 1 of primary visual cortex in the rhesus monkey. Cereb Cortex 2001;11:93–103. [PubMed: 11208664]

Peters A, Rosene DL, Moss MB, Kemper TL, Abraham CR, Tigges J, Albert MS. Neurobiological bases of age-related cognitive decline in the rhesus monkey. J Neuropathol Exp Neurol 1996;55:861–874. [PubMed: 8759775]

Raz N, Gunning FM, Head D, Dupuis JH, McQuain J, Briggs SD, Loken WJ, Thornton AE, Acker JD. Selective aging of the human cerebral cortex observed in vivo: differential vulnerability of the prefrontal gray matter. Cereb Cortex 1997;7:268–282. [PubMed: 9143446]

Raz N, Gunning-Dixon F, Head D, Rodrigue KM, Williamson A, Acker JD. Aging, sexual dimorphism, and hemispheric asymmetry of the cerebral cortex: replicability of regional differences in volume. Neurobiol Aging 2004;25:377–396. [PubMed: 15123343]

Raz N, Lindenberger U, Rodrigue KM, Kennedy KM, Head D, Williamson A, Dahle C, Gerstorf D, Acker JD. Regional brain changes in aging healthy adults: general trends, individual differences and modifiers. Cereb Cortex 2005;15:1676–1689. [PubMed: 15703252]

Ridgway GR, Henley SM, Rohrer JD, Scahill RI, Warren JD, Fox NC. Ten simple rules for reporting voxel-based morphometry studies. Neuroimage 2008;40:1429–1435. [PubMed: 18314353]

Salat DH, Buckner RL, Snyder AZ, Greve DN, Desikan RS, Busa E, Morris JC, Dale AM, Fischl B. Thinning of the cerebral cortex in aging. Cereb Cortex 2004;14:721–730. [PubMed: 15054051]

Saleem, KS.; Logothetis, NK. A Combined MRI and Histology Atlas of the Rhesus Monkey Brain. Academic Press; Amsterdam: 2006.

Sawiak SJ, Wood NI, Williams GB, Morton AJ, Carpenter TA. Voxel-based morphometry in the R6/2 transgenic mouse reveals differences between genotypes not seen with manual 2D morphometry. Neurobiol Dis 2009;33:20–27. [PubMed: 18930824]

Senjem ML, Gunter JL, Shiung MM, Petersen RC, Jack CR Jr. Comparison of different methodological implementations of voxel-based morphometry in neurodegenerative disease. Neuroimage 2005;26:600–608. [PubMed: 15907317]

Sowell ER, Thompson PM, Leonard CM, Welcome SE, Kan E, Toga AW. Longitudinal mapping of cortical thickness and brain growth in normal children. J Neurosci 2004a;24:8223–8231. [PubMed: 15385605]

Sowell ER, Thompson PM, Toga AW. Mapping changes in the human cortex throughout the span of life. Neuroscientist 2004b;10:372–392. [PubMed: 15271264]

Tapp PD, Head K, Head E, Milgram NW, Muggenburg BA, Su MY. Application of an automated voxel-based morphometry technique to assess regional gray and white matter brain atrophy in a canine model of aging. Neuroimage 2006;29:234–244. [PubMed: 16275022]

Tapp PD, Siwak CT, Gao FQ, Chiou JY, Black SE, Head E, Muggenburg BA, Cotman CW, Milgram NW, Su MY. Frontal lobe volume, function, and beta-amyloid pathology in a canine model of aging. J Neurosci 2004;24:8205–8213. [PubMed: 15385603]

Van Essen DC. Surface-based approaches to spatial localization and registration in primate cerebral cortex. Neuroimage 2004;23(Suppl 1):S97–107. [PubMed: 15501104]

Van Essen DC. A Population-Average, Landmark- and Surface-based (PALS) atlas of human cerebral cortex. Neuroimage 2005;28:635–662. [PubMed: 16172003]

Van Essen DC, Dierker DL. Surface-based and probabilistic atlases of primate cerebral cortex. Neuron 2007;56:209–225. [PubMed: 17964241]

Van Essen DC, Drury HA, Dickson J, Harwell J, Hanlon D, Anderson CH. An integrated software suite for surface-based analyses of cerebral cortex. J Am Med Inform Assoc 2001a;8:443–459. [PubMed: 11522765]

Van Essen DC, Lewis JW, Drury HA, Hadjikhani N, Tootell RB, Bakircioglu M, Miller MI. Mapping visual cortex in monkeys and humans using surface-based atlases. Vision Res 2001b;41:1359–1378. [PubMed: 11322980]

Vincent JL, Patel GH, Fox MD, Snyder AZ, Baker JT, Van Essen DC, Zempel JM, Snyder LH, Corbetta M, Raichle ME. Intrinsic functional architecture in the anaesthetized monkey brain. Nature 2007;447:83–86. [PubMed: 17476267]

Wisco JJ, Killiany RJ, Guttmann CR, Warfield SK, Moss MB, Rosene DL. An MRI study of age-related white and gray matter volume changes in the rhesus monkey. Neurobiol Aging. 2007

Wisco JJ, Killiany RJ, Guttmann CR, Warfield SK, Moss MB, Rosene DL. An MRI study of age-related white and gray matter volume changes in the rhesus monkey. Neurobiol Aging 2008;29:1563–1575. [PubMed: 17459528]

Wolf RC, Vasic N, Schonfeldt-Lecuona C, Landwehrmeyer GB, Ecker D. Dorsolateral prefrontal cortex dysfunction in presymptomatic Huntington's disease: evidence from event-related fMRI. Brain 2007;130:2845–2857. [PubMed: 17855375]

Yoo SY, Roh MS, Choi JS, Kang DH, Ha TH, Lee JM, Kim IY, Kim SI, Kwon JS. Voxel-based morphometry study of gray matter abnormalities in obsessive-compulsive disorder. J Korean Med Sci 2008;23:24–30. [PubMed: 18303194]

Zhang Y, Brady M, Smith S. Segmentation of brain MR images through a hidden Markov random field model and the expectation-maximization algorithm. IEEE Trans Med Imaging 2001;20:45–57. [PubMed: 11293691]

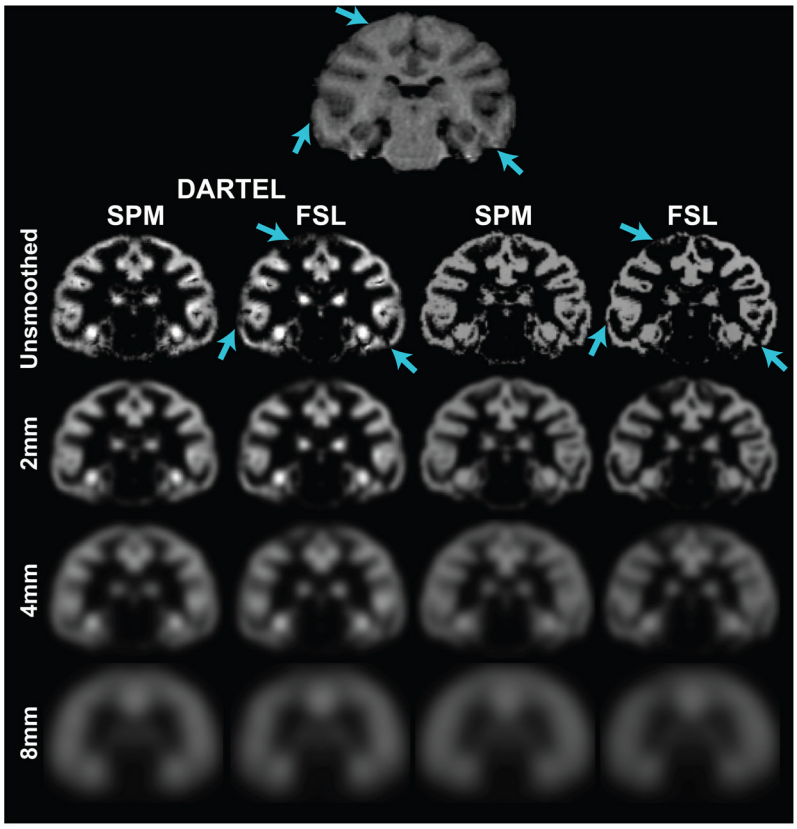

Figure 1.
Segmentation results for one individual processed with all four methods and smoothed with a 2mm, 4mm, and 8mm FWHM Gaussian kernel. Cyan arrows indicate regions that were segmented poorly with FSL compared to SPM.

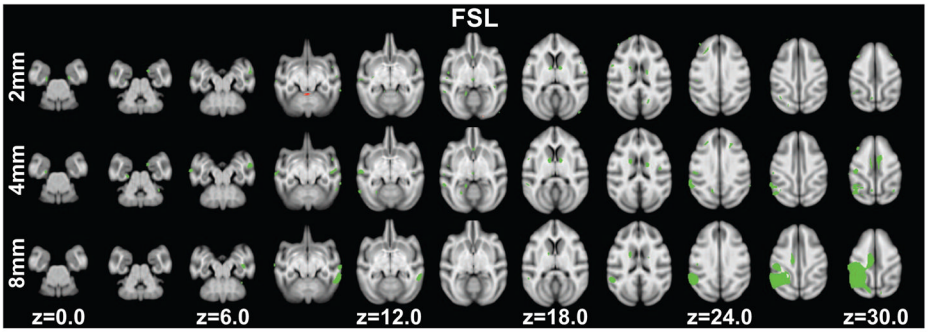

Figure 2.
Significant age-related grey matter volume changes revealed using segments from FSL at $p<0.005$ (uncorrected) in at least 20 edge-connected voxels overlaid on axial slices. Volume increases are shown in red, while decreases are shown in green. Slice positions refer to the 112RM-SL atlas space. Top row: normalized grey matter segments were smoothed with a 2mm FWHM Gaussian kernel. Middle row: normalized grey matter segments were smoothed with a 4mm FWHM Gaussian kernel. Bottom row: normalized grey matter segments were smoothed with an 8mm FWHM Gaussian kernel.

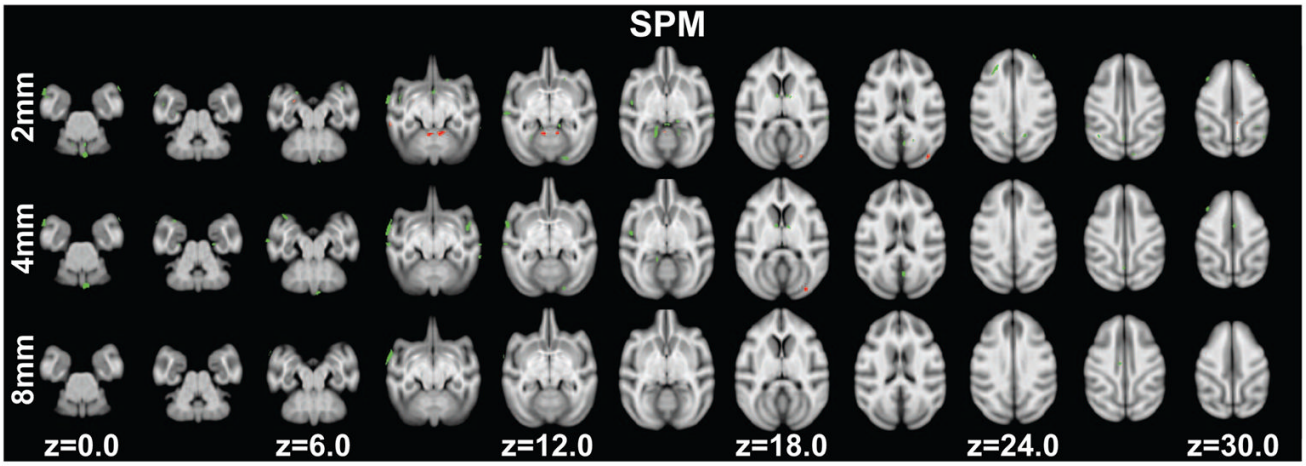

Figure 3.

Significant age-related grey matter changes revealed using unified segmentation in SPM at $p<0.005$ (uncorrected) at least 20 edge-connected voxels overlaid on axial slices. Volume increases are shown in red, while decreases are shown in green. Slice positions refer to the 112RM-SL atlas space. Top row: normalized grey matter segments were smoothed with a 2mm FWHM Gaussian kernel. Middle row: normalized grey matter segments were smoothed with a 4mm FWHM Gaussian kernel. Bottom row: normalized grey matter segments were smoothed with an 8mm FWHM Gaussian kernel.

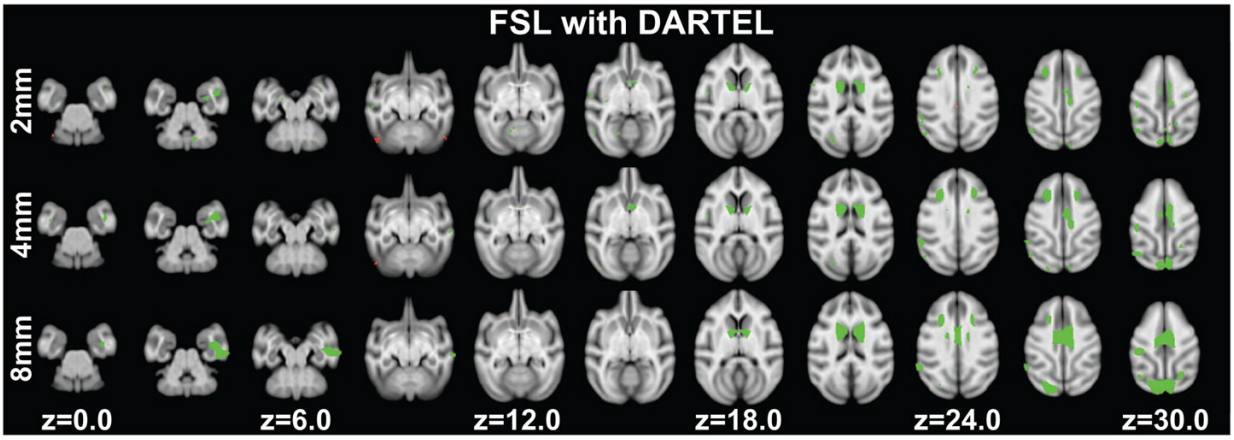

Figure 4.

Significant age-related grey matter changes revealed using DARTEL with segments from FSL at $p<0.005$ (uncorrected) at least 20 edge-connected voxels overlaid on axial slices. Volume increases are shown in red, while decreases are shown in green. Slice positions refer to the 112RM-SL atlas space. Top row: normalized grey matter segments were smoothed with a 2mm FWHM Gaussian kernel. Middle row: normalized grey matter segments were smoothed with a 4mm FWHM Gaussian kernel. Bottom row: normalized grey matter segments were smoothed with an 8mm FWHM Gaussian kernel.

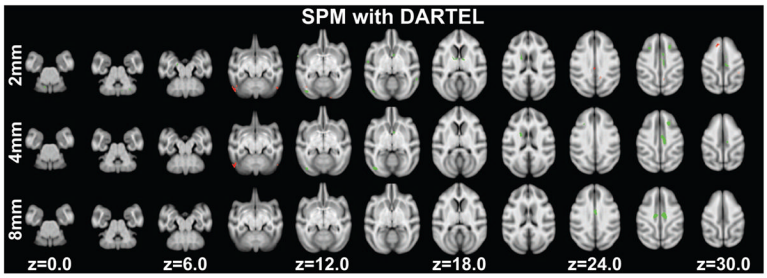

Figure 5.

Significant age-related grey matter changes revealed using DARTEL with output of unified segmentation in SPM at $p<0.005$ (uncorrected) at least 20 edge-connected voxels overlaid on axial slices. Volume increases are shown in red, while decreases are shown in green. Slice positions refer to the 112RM-SL atlas space. Top row: normalized grey matter segments were smoothed with a 2mm FWHM Gaussian kernel. Middle row: normalized grey matter segments were smoothed with a 4mm FWHM Gaussian kernel. Bottom row: normalized grey matter segments were smoothed with an 8mm FWHM Gaussian kernel.